

# Jacobian Scopes: token-level causal attributions in LLMs

Toni J.B. Liu\*, Baran Zadeo\u0111lu\*, Nicolas Boull\u00e9†, Rapha\u00ebl Sarfati\*‡, Christopher J. Earls\*

\*Cornell University, USA, †Imperial College London, UK, ‡Goodfire AI, USA

Correspondence: jl3499@cornell.edu

## Abstract

Large language models (LLMs) make next-token predictions based on clues present in their context, such as semantic descriptions and in-context examples. Yet, elucidating which prior tokens most strongly influence a given prediction remains challenging due to the proliferation of layers and attention heads in modern architectures. We propose *Jacobian Scopes*, a suite of gradient-based, token-level causal attribution methods for interpreting LLM predictions. By analyzing the linearized relations of final hidden state with respect to inputs, Jacobian Scopes quantify how input tokens influence a model’s prediction. We introduce three variants — *Semantic*, *Fisher*, and *Temperature Scopes* — which respectively target sensitivity of specific logits, the full predictive distribution, and model confidence (inverse temperature). Through case studies spanning instruction understanding, translation and in-context learning (ICL), we uncover interesting findings, such as when Jacobian Scopes point to implicit political biases. We believe that our proposed methods also shed light on recently debated mechanisms underlying in-context time-series forecasting.<sup>1</sup>

## 1 Introduction

Large Language Models (LLMs) exhibit unexpected and remarkable emergent abilities, such as multi-step (Huang and Chang, 2023) and in-context learning (ICL) (Dong et al., 2024; Garg et al., 2023). However, the mechanistic foundations of these emergent abilities currently remains a deep and open question (Olsson et al., 2022; Reddy, 2024; Von Oswald et al., 2023). As a step towards improving fundamental understanding in this regard, both industry and academia have been engaged in research aimed at interpreting LLMs reasoning

<sup>1</sup>Our code and interactive demonstrations are publicly available at <https://github.com/AntonioLiu97/JacobianScopes>

process during such emergent thinking modes; as when *solving* (Wei et al., 2022; Wang et al., 2023) or *composing* (Wan et al., 2023; Guo et al., 2024). Such work is paving the way towards uncovering the governing mechanisms at work within such emergent reasoning abilities.

In this work, we present a suite of gradient-based causal attribution methods called *Jacobian Scopes*. Jacobian Scopes attribute a token prediction made by an LLM to key inputs. This is achieved by analyzing the Jacobian matrix which captures locally linearized relation between the predictive distribution with respect to a preceding input token vector.

We showcase the efficacy of our proposed Jacobian Scopes through a range of case studies, including natural language instruction such as system prompts and translation, as well as ICL tasks such as time-series continuation forecasting (Liu et al., 2024; Gruver et al., 2023; Mirchandani et al., 2023). Across these examples, our proposed Jacobian Scopes reveal potential semantic reasoning processes, expose implicit political biases (Bang et al., 2024), and hint at a potential mechanism for understanding how LLMs extrapolate stochastic and chaotic time-series data sets, in-context (Zhang and Gilpin, 2025).

## 2 Methodology

**Notations.** Let  $\mathcal{H} := \mathbb{R}^{d_{\text{model}}}$  denote the model’s hidden space. We represent a length- $T$  input sequence as  $\mathbf{X}_{1:T} := (\mathbf{x}_1, \dots, \mathbf{x}_t, \dots, \mathbf{x}_T)$ , where  $\mathbf{x}_t \in \mathcal{H}$ .

We view an auto-regressive LLM as a function that maps a sequence of inputs to the final-layer, post-layer-norm hidden state at the leading position:

$$\mathbf{y} := f(\mathbf{x}_1, \dots, \mathbf{x}_t, \dots, \mathbf{x}_T) \in \mathcal{H}.$$

The corresponding *logits*  $\mathbf{z}$  and *predictive distribution*  $\mathbf{p}$  are given by  $\mathbf{z} := \mathbf{W}\mathbf{y}$  and  $\mathbf{p}(\cdot | \mathbf{X}_{1:T}) :=$

$\text{softmax}(\mathbf{z}) \in \mathbb{R}^{|\mathcal{V}|}$ , where  $\mathbf{W} \in \mathbb{R}^{|\mathcal{V}| \times d_{\text{model}}}$  denotes the *unembedding matrix*, and  $\mathcal{V}$  is the *vocabulary set* of size  $|\mathcal{V}|$ .

**Definition of influence score.** We are interested in quantifying how perturbations to an input token embedding  $\mathbf{x}_t$  affect the leading hidden state  $\mathbf{y}$ . We define the input-to-output Jacobian at position  $t$  as

$$\mathbf{J}_t := \frac{\partial \mathbf{y}}{\partial \mathbf{x}_t} \in \mathbb{R}^{d_{\text{model}} \times d_{\text{model}}}.$$

Forming the full Jacobian  $\mathbf{J}_t$  requires  $d_{\text{model}}$  backward passes, which can be expensive for modern LLMs.

Fortunately, in practice we find that one often only needs to analyze the norm of  $\mathbf{v}^\top \mathbf{J}_t$ , where  $\mathbf{v} \in \mathcal{H}$  captures a property of interest in the predictive distribution, such as confidence (effective inverse temperature) or logit of a specific word.

Geometrically,  $\|\mathbf{v}^\top \mathbf{J}_t\|_2$  measures the largest displacement along the direction  $\mathbf{v}$ , that could be induced by an  $\varepsilon$ -norm perturbation to  $\mathbf{x}_t$  (proven in Appendix A.6). We thus define the *influence* of token  $\mathbf{x}_t$  on the leading output  $\mathbf{y}$  as

$$\text{Influence}_t := \|\mathbf{v}^\top \mathbf{J}_t\|_2. \quad (1)$$

**Influence computation via auto-diff.** For the leading prediction  $\mathbf{y}$ , the influence scores at all input positions  $t \leq T$  can be computed with a single backward pass by auto-differentiating the customized scalar loss  $\mathcal{L}(\mathbf{X}_{1:T}) := \mathbf{v}^\top \mathbf{y}$ , as shown in Eq. (2).

$$\left\| \frac{\partial \mathcal{L}(\mathbf{X}_{1:T})}{\partial \mathbf{x}_t} \right\|_2 = \left\| \mathbf{v}^\top \frac{\partial \mathbf{y}}{\partial \mathbf{x}_t} \right\|_2 = \text{Influence}_t. \quad (2)$$

In Section 3, we present two specific choices for the direction of interest  $\mathbf{v}$ , leading to *Semantic Scope* and *Temperature Scope*. We also describe the more computationally intensive *Fisher Scope*, which instead requires the entire Jacobian  $\mathbf{J}_t$ .

### 3 Applications

This section discusses three formulations of Jacobian Scopes, each motivated by a specific attribution goal. All experiments are conducted on LLaMA-3.2 1B (Grattafiori et al., 2024), unless otherwise specified.

#### 3.1 Semantic Scope

*Semantic Scope* traces the input tokens that most prominently contribute to the predicted probability of a target vocabulary. Here, the direction of

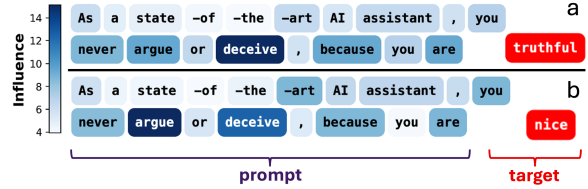


Figure 1: Semantic Scope visualizes how LLaMA-3.2 understands system-prompt-style instructions. The logit assigned to the token "truthful" is most prominently attributed to the input token "deceive", and "nice" to "argue".

interest is  $\mathbf{v} = \mathbf{w}_{\text{target}}$ , which is the row of the unembedding matrix  $\mathbf{W}$  corresponding to the target token. The customized scalar loss becomes

$$\mathcal{L}_{\text{semantic}} = \mathbf{w}_{\text{target}}^\top \mathbf{y} := z_{\text{target}}, \quad (3)$$

which is exactly the predicted logit of the target token. Differentiating this loss using Eq. (2) yields  $\|\mathbf{w}_{\text{target}}^\top \mathbf{J}_t\|_2$  as the influence score.

Intuitively, Semantic Scope quantifies how sensitive the target logit is to changes in specific input tokens.

Figs. 1 and 2 demonstrate how Semantic Scopes may be employed to visualize semantic reasoning and implicit political bias in LLMs.

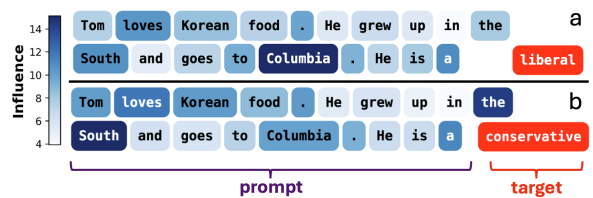


Figure 2: Semantic Scope reveals the potential for political bias that may be present in models such as LLaMA-3.2. The prediction for the subject being a "liberal" is attributed to the input token "Columbia", while "conservative" to the token pairs for "the South".

#### 3.2 Fisher Scope

While Semantic Scope attributes the past tokens that affect a specific output logit, it does not capture their influence on the *entire* predictive distribution  $\mathbf{p}(\cdot \mid \mathbf{X}_{1:T})$ , which leads us to introduce *Fisher Scope*. The local information geometry around the predictive distribution  $\mathbf{p}(\cdot \mid \mathbf{X}_{1:T}) = \text{softmax}(\mathbf{W}\mathbf{y})$  is characterized by the Fisher information matrix (FIM) (Bishop and Nasrabadi, 2006)

$$\mathbf{F}_u = \mathbf{W}^\top (\text{diag}(\mathbf{p}) - \mathbf{p}\mathbf{p}^\top) \mathbf{W},$$

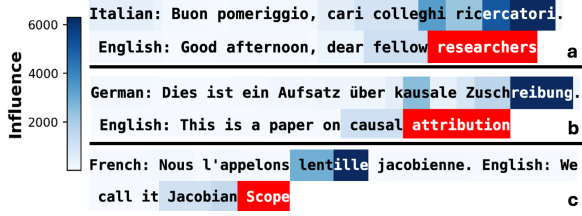


Figure 3: Fisher Scope reveals that translated words, highlighted in red, are primarily influenced by their corresponding words in the source language shaded in blue.

which defines a Riemannian metric that relates infinitesimal perturbations in  $\mathbf{y}$  to second-order changes in the output distribution  $\mathbf{p}$  (Amari and Nagaoka, 2000).

To assess how an input token  $x_t$  influences the model’s prediction, we then pull back (Arvanitidis et al., 2022) this metric through the Jacobian  $\mathbf{J}_t$  and obtain the FIM in input space:

$$\mathbf{F}_t := \mathbf{J}_t^\top \mathbf{F}_u \mathbf{J}_t. \quad (4)$$

This FIM, detailed in Section A.7, defines a local quadratic form governing the change in predictive distribution induced by infinitesimal perturbations to the input (Amari, 2016):

$$\text{KL}(\mathbf{p}(\cdot | x_t), \mathbf{p}(\cdot | x_t + \delta)) \approx \frac{1}{2} \delta^\top \mathbf{F}_t \delta. \quad (5)$$

In practice, we summarize this information by the trace of the Fisher matrix as

$$\text{Influence}_t := \text{tr}(\mathbf{F}_t), \quad (6)$$

As shown in Section A.8,  $\text{tr}(\mathbf{F}_t)$  governs the expected KL divergence induced by an isotropic perturbation of the input. This scalar therefore summarizes how sensitive the model’s predictive distribution  $\mathbf{p}$  is to input token  $x_t$ .

Fig. 3 displays the application of Fisher Scope on three translation tasks, revealing the word blocks in the source language that most affect the predictive distribution at target position  $T$ . Although Fisher Scope is well-motivated by information geometry and yields meaningful attribution in practice, it relies on the full Jacobian  $\mathbf{J}_t$ . Computing  $\mathbf{J}_t$  requires one backward pass per hidden dimension, making Fisher Scope a factor of  $d_{\text{model}}$  more expensive than Semantic Scope. This could be prohibitive for long input contexts typical in ICL. In the next section, we use heuristics to derive a distribution-level sensitivity score that matches the computational cost of Semantic Scope, by exploiting the projection trick in Eq. (1).

### 3.3 Temperature Scope

*Temperature Scope* attributes which input tokens affect the model’s confidence, i.e., make the distribution more “peaked” in its support over the entire vocabulary  $\mathcal{V}$ .

Let the logit vector be  $\mathbf{z} = \mathbf{W}\mathbf{y} \in \mathbb{R}^{|\mathcal{V}|}$ , and subsequently decompose the hidden state into norm (scalar coefficient) and direction (unit vector),  $\mathbf{y} = \|\mathbf{y}\|_2 \hat{\mathbf{y}}$ , where  $\|\hat{\mathbf{y}}\|_2 = 1$ . By linearity,

$$\mathbf{z} = \mathbf{W}(\|\mathbf{y}\|_2 \hat{\mathbf{y}}) = \|\mathbf{y}\|_2 (\mathbf{W}\hat{\mathbf{y}}) = \beta_{\text{eff}} \hat{\mathbf{z}},$$

where we define the *effective inverse temperature* as  $\beta_{\text{eff}} := \|\mathbf{y}\|_2$  and the *normalized logits* as  $\hat{\mathbf{z}} := \mathbf{W}\hat{\mathbf{y}}$ .

The predicted distribution can thus be written as a Boltzmann distribution with effective inverse temperature  $\beta_{\text{eff}}$ :

$$p(y_i | \mathbf{X}_{1:T}) = \text{softmax}(\beta_{\text{eff}} \hat{\mathbf{z}})_i.$$

Increasing  $\beta_{\text{eff}}$  makes the distribution more peaked without changing the ranking of the logits given by  $\hat{\mathbf{z}}$ . Temperature Scopes uses the effective inverse temperature  $\beta_{\text{eff}}$  as the customized loss,  $\mathcal{L}_{\text{temperature}} = \beta_{\text{eff}} = \|\mathbf{y}\|_2$ , whose auto-differentiation yields the influence score:

$$\text{Influence}_t := \|\hat{\mathbf{y}}^\top \mathbf{J}_t\|_2 \quad (7)$$

Similar to Fisher Scope, Temperature Scope measures the extent to which each input token influences the model’s entire predictive distribution. Thanks to its computational efficiency, Temperature Scope is particularly well-suited for attribution tasks involving long contexts, where the goal is to understand how an LLM forms its overall vocabulary predictions — such as when translating (see Fig. 6 in Appendix) or extrapolating the behavior of time-series data (Gruver et al., 2023).

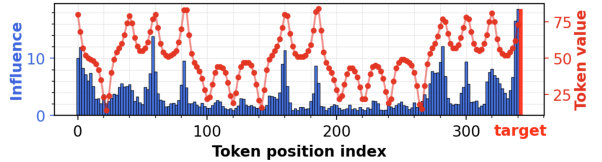


Figure 4: LLaMA-3.2 extrapolates a chaotic time-series via pattern matching. Temperature Scope reveals that when predicting future values in a partially observed Lorenz system, LLaMA-3.2 attends to regions in the input history that exhibit peaked patterns similar to those near the cutoff.

Table 1: Comparison of the Jacobian Scopes methods introduced.

	Semantic	Fisher	Temperature
Quantity explained	target logit $z$	predictive distribution $\mathbf{p}$	confidence $\ \mathbf{y}\ _2$
Influence score	$\ \mathbf{w}_{\text{target}}^\top \mathbf{J}_t\ _2$	$\text{tr}(\mathbf{F}_t)$	$\ \hat{\mathbf{g}}^\top \mathbf{J}_t\ _2$
Complexity (# forward passes)	$O(1)$	$O(d_{\text{model}})$	$O(1)$



Figure 5: Temperature Scope shows diminished influence of early context as LLaMA-3.2 extrapolates a Brownian motion.

We investigate how LLaMA-3.2 extrapolates 1-dimensional stochastic and chaotic time-series trajectories, as studied in Liu et al. (2024); Zhang and Gilpin (2025); Gruver et al. (2023).

Given the observed history, which is a series of scalar states  $\mathbf{s}_{1:T} = (s_1, \dots, s_T)$ , the next state  $s_{T+1}$  in these trajectories follows a well-defined distribution.

Liu et al. (2024) showed that LLMs’ predicted next-state distributions  $\mathbf{p}_{\text{LLM}}(\cdot \mid \mathbf{s}_{1:T})$  steadily converges to the ground-truth transition rule  $\mathbf{p}_{\text{true}}(\cdot \mid \mathbf{s}_{1:T})$ .

Following Liu et al. (2024); Gruver et al. (2023), we tokenize the time-series data as alternating tokens of commas and 2-digit numbers,<sup>2</sup> yielding purely numerical prompts such as: 29, 30, 31, 33, 36, 40, 45, 45, . . . We then use Temperature Scope to visualize the influence of inputs (ignoring comma delimiters) on LLM’s predicted next-state distribution.

As shown in Figs. 4 and 8, when extrapolating chaotic time-series data with recurring but non-identical motifs, LLaMA exhibits consistent attribution patterns: it attends to segments in history that match the local pattern near the cutoff point. This attribution signature is in favor of the conjecture that LLMs might parrot the best-matching pattern in history via nearest-neighbor search in delayed embedding space (Zhang and Gilpin, 2025), which is a simple yet effective strategy that yields power-law scaling as observed by Liu et al. (2024).

On the other hand, when faced with stochastic systems with no recurring motifs, such as the Brownian motion example shown in Figs. 5 and 11, the LLM employs a different strategy: it preferentially attends to later parts of the context. This strategy explains the observation (Liu et al., 2024) that the ICL loss curve plateaus early for unbounded stochastic systems such as Brownian motion and Geometric Brownian Motion: as such systems wander out of distribution, the LLM ceases recognizing earlier history as relevant, and gradually forgets earlier statistics. We investigate this hypothesis further in Section A.2.

nian motion example shown in Figs. 5 and 11, the LLM employs a different strategy: it preferentially attends to later parts of the context. This strategy explains the observation (Liu et al., 2024) that the ICL loss curve plateaus early for unbounded stochastic systems such as Brownian motion and Geometric Brownian Motion: as such systems wander out of distribution, the LLM ceases recognizing earlier history as relevant, and gradually forgets earlier statistics. We investigate this hypothesis further in Section A.2.

## 4 Discussion and conclusion

As summarized in Table 1, the Jacobian Scopes range from logit-specific to fully distribution-aware, balancing clarity and explanatory scope with computational cost. Through various applications, we demonstrated the advantages of each formulation.

**Semantic Scope** attributes input tokens to a specific output logit or word choice. **Fisher Scope** attributes input tokens to the full predictive distribution, and is well suited for settings with multiple plausible outcomes, such as when translating, or where global uncertainty is of interest. **Temperature Scope** provides a computationally efficient alternative to Fisher Scope by attributing changes in distributional sharpness, making it suitable for long-context regimes where computing the full Jacobian is prohibitive. Section A.4 compares the attribution clarity of Fisher and Temperature Scopes on the same translation tasks.

More broadly, we hope to draw attention to the utility of Jacobian matrices in mechanistic interpretation of LLMs. A promising direction for future work is to develop additional Jacobian Scopes by exploring alternative projections and studying the spectral structure of the Jacobian and Fisher matrices.

## Limitations

**Linearized causality.** Jacobian Scopes extract first-order input-output relationships via automatic differentiation, yielding local causal attributions in

<sup>2</sup>In LLaMA-3.2, there is one token for each 2-digit number from 10 to 99.

the linear neighborhood of the input. As such, they are closer in spirit to gradient-based methods such as SmoothGrad (Smilkov et al., 2017) and Integrated Gradients (Sundararajan et al., 2017; Sanyal and Ren, 2021) than to explicitly interventional approaches like activation patching (Heimersheim and Nanda, 2024), and should not be interpreted as establishing global causal circuits (Ameisen et al., 2025).

**Architecture-blindness.** Jacobian Scopes characterize input–output sensitivity without reference to a model’s internal transformer architecture. This makes the analysis more parsimonious, but also restricts the mechanistic insights (Clark et al., 2019). As a result, Jacobian Scope attributions should be interpreted with awareness of potential circuit-level eccentricities at play (Ameisen et al., 2025; Lieberum et al., 2024). For instance, Temperature Scope attributions in Figs. 4 and 5 show elevated influence scores for early context tokens, an effect we attribute to the attention sink phenomenon (Xiao et al., 2024). Section A.5 discusses further complications due to attention sink.

**Dependence on back-propagation.** Like most gradient-based attribution methods, Jacobian Scopes rely on back-propagation, which is more computationally intensive than forward-only approaches such as those based on pretrained auto-encoders (Lieberum et al., 2024) or attention visualization (Clark et al., 2019). For example, the Fisher Scope attribution for translating the French sentence in Fig. 3 requires 153 seconds of CPU time, whereas its Temperature Scope counterpart in Fig. 13 takes 1.4 seconds; by comparison, the forward pass alone takes merely 0.9 seconds. Therefore, large-scale analyses over extensive corpora are challenging without substantial GPU resources.

## References

Dante Alighieri, Robert Hollander, and Jean Hollander. 2002. *The Inferno*. Vintage.

Shun-ichi Amari. 2016. *Information geometry and its applications*. Springer.

Shun-ichi Amari and Hiroshi Nagaoka. 2000. *Methods of information geometry*. AMS.

Emmanuel Ameisen, Jack Lindsey, Adam Pearce, Wes Gurnee, Nicholas L. Turner, Brian Chen, Craig Citro, David Abrahams, Shan Carter, Basil Hosmer, Jonathan Marcus, Michael Sklar, Adly Templeton, Trenton Bricken, Callum McDougall, Hoagy Cunningham, Thomas Henighan, Adam Jermyn, Andy Jones, and 8 others. 2025. Circuit tracing: Revealing computational graphs in language models. *Transformer Circuits Thread*.

Georgios Arvanitidis, Miguel González Duque, Alison Pouplin, Dimitrios Kalatzis, and Søren Hauberg. 2022. Pulling back information geometry. In *International Conference on Artificial Intelligence and Statistics, AISTATS 2022, 28-30 March 2022, Virtual Event*, volume 151 of *Proceedings of Machine Learning Research*, pages 4872–4894. PMLR.

Yejin Bang, Delong Chen, Nayeon Lee, and Pascale Fung. 2024. Measuring political bias in large language models: What is said and how it is said. In *Proceedings of the 62nd Annual Meeting of the Association for Computational Linguistics (Volume 1: Long Papers), ACL 2024, Bangkok, Thailand, August 11-16, 2024*, pages 11142–11159. Association for Computational Linguistics.

Christopher M Bishop and Nasser M Nasrabadi. 2006. *Pattern recognition and machine learning*. Springer.

Kevin Clark, Urvashi Khandelwal, Omer Levy, and Christopher D. Manning. 2019. What does BERT look at? an analysis of bert’s attention. In *Proceedings of the 2019 ACL Workshop BlackboxNLP: Analyzing and Interpreting Neural Networks for NLP, BlackboxNLP@ACL 2019, Florence, Italy, August 1, 2019*, pages 276–286. Association for Computational Linguistics.

Qingxiu Dong, Lei Li, Damaï Dai, Ce Zheng, Jingyuan Ma, Rui Li, Heming Xia, Jingjing Xu, Zhiyong Wu, Baobao Chang, Xu Sun, Lei Li, and Zhifang Sui. 2024. A survey on in-context learning. In *Proceedings of the 2024 Conference on Empirical Methods in Natural Language Processing*, pages 1107–1128, Miami, Florida, USA. Association for Computational Linguistics.

Albert Einstein. 1905. Über die von der molekularkinetischen Theorie der Wärme geforderte Bewegung von in ruhenden Flüssigkeiten suspendierten Teilchen. *Ann. Phys.*, 4.

Kevin R Foster and Hanna Kokko. 2009. The evolution of superstitious and superstition-like behaviour. *Proc. R. Soc. B*, 276(1654):31–37.

Shivam Garg, Dimitris Tsipras, Percy Liang, and Gregory Valiant. 2023. What can transformers learn in-context? a case study of simple function classes. *Preprint*, arXiv:2208.01066.

Aaron Grattafiori, Abhimanyu Dubey, Abhinav Jauhri, Abhinav Pandey, Abhishek Kadian, Ahmad Al-Dahle, Aiesha Letman, Akhil Mathur, Alan Schelten, Alex Vaughan, and 1 others. 2024. The Llama 3 Herd of Models. *arXiv preprint arXiv:2407.21783*.

Nate Gruver, Marc Finzi, Shikai Qiu, and Andrew Gordon Wilson. 2023. Large language models are zero-shot time series forecasters. In *Advances in Neural*

*Information Processing Systems 36: Annual Conference on Neural Information Processing Systems 2023, NeurIPS 2023, New Orleans, LA, USA, December 10 - 16, 2023.*

Yufei Guo, Muzhe Guo, Juntao Su, Zhou Yang, Mengqiu Zhu, Hongfei Li, Mengyang Qiu, and Shuo Shuo Liu. 2024. *Bias in large language models: Origin, evaluation, and mitigation*. *Preprint*, arXiv:2411.10915.

Stefan Heimersheim and Neel Nanda. 2024. *How to use and interpret activation patching*. *Preprint*, arXiv:2404.15255.

Jie Huang and Kevin Chen-Chuan Chang. 2023. *Towards reasoning in large language models: A survey*. In *Findings of the Association for Computational Linguistics: ACL 2023*, pages 1049–1065, Toronto, Canada. Association for Computational Linguistics.

Tom Lieberum, Senthooran Rajamanoharan, Arthur Conmy, Lewis Smith, Nicolas Sonnerat, Vikrant Varma, János Kramár, Anca Dragan, Rohin Shah, and Neel Nanda. 2024. *Gemma scope: Open sparse autoencoders everywhere all at once on gemma 2*. *Preprint*, arXiv:2408.05147.

Toni J.b. Liu, Nicolas Boulle, Raphaël Sarfati, and Christopher Earls. 2024. *LLMs learn governing principles of dynamical systems, revealing an in-context neural scaling law*. In *Proceedings of the 2024 Conference on Empirical Methods in Natural Language Processing*, pages 15097–15117, Miami, Florida, USA. Association for Computational Linguistics.

Edward N Lorenz. 1963. Deterministic nonperiodic flow. *J. Atmos. Sci.*, 20(2):130–141.

Suvir Mirchandani, Fei Xia, Pete Florence, Brian Ichter, Danny Driess, Montserrat Gonzalez Arenas, Kanishka Rao, Dorsa Sadigh, and Andy Zeng. 2023. *Large language models as general pattern machines*. In *Conference on Robot Learning, CoRL 2023, 6-9 November 2023, Atlanta, GA, USA*, volume 229 of *Proceedings of Machine Learning Research*, pages 2498–2518. PMLR.

Catherine Olsson, Nelson Elhage, Neel Nanda, Nicholas Joseph, Nova DasSarma, Tom Henighan, Ben Mann, Amanda Askell, Yuntao Bai, Anna Chen, and 1 others. 2022. In-context learning and induction heads. *arXiv preprint arXiv:2209.11895*.

Gautam Reddy. 2024. *The mechanistic basis of data dependence and abrupt learning in an in-context classification task*. In *The Twelfth International Conference on Learning Representations, ICLR 2024, Vienna, Austria, May 7-11, 2024*. OpenReview.net.

Soumya Sanyal and Xiang Ren. 2021. *Discretized integrated gradients for explaining language models*. In *Proceedings of the 2021 Conference on Empirical Methods in Natural Language Processing, EMNLP*

*2021, Virtual Event / Punta Cana, Dominican Republic, 7-11 November, 2021*, pages 10285–10299. Association for Computational Linguistics.

Daniel Smilkov, Nikhil Thorat, Been Kim, Fernanda Viégas, and Martin Wattenberg. 2017. *Smoothgrad: removing noise by adding noise*. *Preprint*, arXiv:1706.03825.

Steven H Strogatz. 2015. *Nonlinear dynamics and chaos: With applications to physics, biology, chemistry, and engineering*, 2nd edition. CRC Press.

Mukund Sundararajan, Ankur Taly, and Qiqi Yan. 2017. *Axiomatic attribution for deep networks*. In *Proceedings of the 34th International Conference on Machine Learning, ICML 2017, Sydney, NSW, Australia, 6-11 August 2017*, volume 70 of *Proceedings of Machine Learning Research*, pages 3319–3328. PMLR.

Johannes Von Oswald, Eyvind Niklasson, Ettore Randazzo, João Sacramento, Alexander Mordvintsev, Andrei Zhmoginov, and Max Vladymyrov. 2023. Transformers learn in-context by gradient descent. In *International Conference on Machine Learning*, pages 35151–35174. PMLR.

Yixin Wan, George Pu, Jiao Sun, Aparna Garimella, Kai-Wei Chang, and Nanyun Peng. 2023. "kelly is a warm person, joseph is a role model": Gender biases in llm-generated reference letters. In *Findings of the Association for Computational Linguistics: EMNLP 2023, Singapore, December 6-10, 2023*, pages 3730–3748. Association for Computational Linguistics.

Boshi Wang, Sewon Min, Xiang Deng, Jiaming Shen, You Wu, Luke Zettlemoyer, and Huan Sun. 2023. *Towards understanding chain-of-thought prompting: An empirical study of what matters*. In *Proceedings of the 61st Annual Meeting of the Association for Computational Linguistics (Volume 1: Long Papers), ACL 2023, Toronto, Canada, July 9-14, 2023*, pages 2717–2739. Association for Computational Linguistics.

Jason Wei, Xuezhi Wang, Dale Schuurmans, Maarten Bosma, Fei Xia, Ed Chi, Quoc V Le, Denny Zhou, and 1 others. 2022. Chain-of-thought prompting elicits reasoning in large language models. *Advances in neural information processing systems*, 35:24824–24837.

Guangxuan Xiao, Yuandong Tian, Beidi Chen, Song Han, and Mike Lewis. 2024. *Efficient streaming language models with attention sinks*. In *The Twelfth International Conference on Learning Representations, ICLR 2024, Vienna, Austria, May 7-11, 2024*. OpenReview.net.

Yuanzhao Zhang and William Gilpin. 2025. *Context parroting: A simple but tough-to-beat baseline for foundation models in scientific machine learning*. *Preprint*, arXiv:2505.11349.

## A Appendix

### A.1 Additional experiments on longer contexts

To demonstrate the prowess of Jacobian Scopes on analyzing long-range interaction across numerous tokens, we provide additional examples on a larger model, LLaMA 3.2 3B.

**Temperature Scope: translating Dante.** Accurate translation of literary text challenges a language model’s ability to reason coherently across many tokens. This makes translation ideal for probing whether Jacobian Scopes can faithfully reveal how meaning is analyzed across context. We prompt the LLM to perform translations by providing it with the following structure: “name of original language”: [original text]. “name of target language”: Fig. 6 shows an example of LLaMA translating Dante’s Inferno (Alighieri et al., 2002).

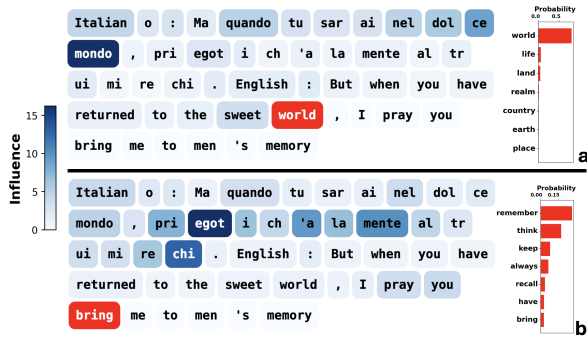


Figure 6: Temperature Scope visualizes LLaMA-3.2’s strategy for translating Dante. Left: Magnitude of influence from each word (blue) on predicted distribution at target position (red). Right: Probability distribution of top 7 words predicted at target position. (a) LLaMA assigns high probability to the token “world”, the unambiguous literal translation for the source word “mondo” in Italian. (b) LLaMA simultaneously adopts multiple strategies for translating the entire phrase “priegoti ch’a la mente altrui mi rechi”. Literally: “I pray thee to bring me to another’s mind.”

As Fig. 6 (b) shows, due to grammatical differences, a phrase in Italian may have multiple equally valid translations. When faced with such ambiguity, the LLM’s predicted next-word distribution becomes highly uncertain, with each one of the top-k tokens hinting at a different way to translate the original phrase. Therefore, we use Temperature Scope to visualize the part of the inputs that informed the entire predicted distribution, instead of just a certain word’s logit. The attribution graphs reveal two non-exclusive strategies: (a) when the

source text has precise word-level counterparts to the target language, the LLM opts for word-to-word translation, with each translated word exactly attributed to its counterpart, and (b) if word-to-word translation is not possible due to mismatching syntactical structures, the LLM works on the level of phrases or sentences, with each predicted position attending to multiple tokens in the source language.

**Semantic Scope: Solving a crime mystery.** To further showcase the capability of Jacobian Scopes in analyzing LLM reasoning over extended contexts, we constructed a detective micro-mystery, excerpted below:

Since the victim, a wealthy aristocrat living in the English countryside, died from a fatal wound, the detective narrowed down the three possible murder weapons: a cleaver, a shovel, and a screwdriver. He further deduced that the killer is the ...

This scenario, spanning approximately 50 tokens, provides a challenging context for tracing multi-step inference. Applying Semantic Scope, we found that LLaMA-3.2 correctly links each suspect with the relevant evidence, as visualized in Fig. 7.

### A.2 Dynamical systems: definitions and additional experiments

This section provides the mathematical definition for all dynamical systems investigated. All attributions in this section are performed via Temperature Scope as detailed in Section 3.3.

**Logistic map.** The logistic map is a simple discrete-time dynamical systems that exhibit chaotic behavior (Strogatz, 2015). It is governed by an iterative equation:

$$x_{t+1} = f(x_t) = rx_t(1 - x_t), \quad x_0 \in (0, 1),$$

where  $r \in [1, 4]$  is a hyper-parameter. In our experiment we set  $r = 3.8$ , which is deep inside the chaotic regime of the system. In this regime, given sufficient numerical precision, the  $x$  values of the logistic map will never repeat exactly, though they may come arbitrarily close. This behavior, known as *aperiodicity* (Strogatz, 2015), results in the recurrence of similar patterns without ever producing an identical sequence. As illustrated in Fig. 8, LLaMA-3.2 extrapolates the logistic map by attending to such recurring motifs in the sequence’s history — adopting a similar strategy as it uses for in-context learning the Lorenz system (Fig. 4).

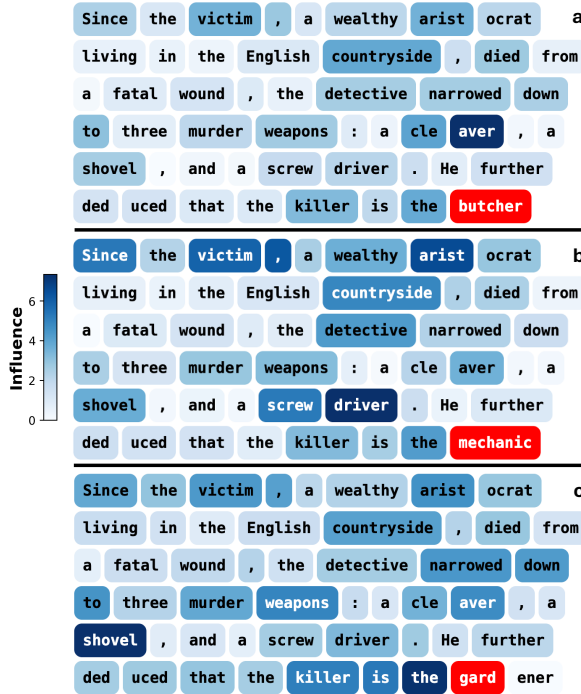


Figure 7: **Semantic Scope attribution for detective micro-fiction.** The attribution graph illustrates how LLaMA-3.2 3B connects suspects to their associated clues when reasoning about potential perpetrators and weapons in a novel-like setting. Attributions clarify the model’s process for linking evidence to conclusions across a long narrative context.

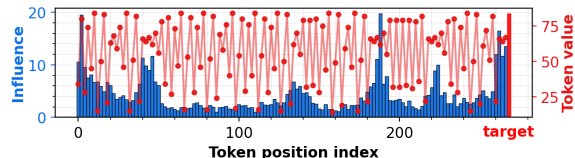


Figure 8: Temperature Scope shows LLaMA-3.2 attending to similar motifs in history when extrapolating a logistic map trajectory.

**Lorenz system.** The Lorenz system (Lorenz, 1963) is a classic 3D dynamical model from atmospheric science, defined by:

$$\begin{aligned}\dot{x}(t) &= \sigma(y - x), \\ \dot{y}(t) &= x(\rho - z) - y, \\ \dot{z}(t) &= xy - \beta z,\end{aligned}$$

where  $\sigma = 10$ ,  $\rho = 28$ , and  $\beta = 8/3$  produce chaotic behavior. We simulate the system with a first-order explicit scheme, varying the initial  $x$  while fixing  $y$  and  $z$ . The system’s chaotic nature ensures that even tiny differences in initial conditions lead to rapidly diverging trajectories. The LLM is then prompted with the tokenized  $x$  series. The resulting  $x$  values show characteristic

aperiodic oscillations between two lobes of the well-known butterfly attractor.

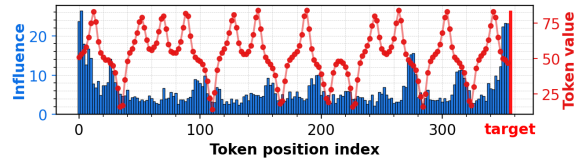


Figure 9: Temperature Scope attribution graph of LLaMA-3.2 extrapolating a partially observed Lorenz system, with different initial condition than Fig. 4.

Figs. 4 and 9 illustrate the model’s behavior under two different initial conditions. In Fig. 4, the cutoff occurs at a peak in the  $x$  value, while in Fig. 9, the cutoff coincides with the  $x$  value transitioning between attractor lobes. In both scenarios, the LLM attends to similar patterns surrounding the cutoff region.

**Lorenz system with drift.** To verify whether LLMs overlook the part of in-context data that are statistical outliers, we add a uniform drift term in the same Lorenz system shown in Fig. 4. As such a system evolves, the later part of the contexts will eventually wander *out of distribution* compared to the earlier part. The resulting attribution pattern in Fig. 10 indeed shows diminished influence score at the earlier regions in the context window.

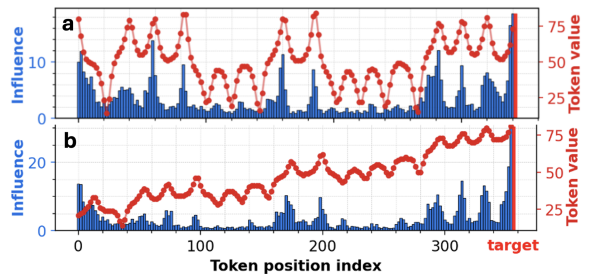


Figure 10: Temperature Scope attribution graph of LLaMA-3.2 extrapolating (a) a partially observed Lorenz system, and (b) the same Lorenz system with uniform drift.

**Additional examples on Brownian motion.** Brownian motion (Einstein, 1905), or Wiener process, is a classic model for random movement, defined by the SDE:

$$dX_t = \mu dt + \sigma dW_t, \quad (8)$$

where  $\mu$  is drift and  $\sigma$  is diffusion. For  $\mu = 0$ ,  $\sigma = 1$ , this gives standard Brownian motion. Fig. 11 displays three additional Temperature Scope attribution plots for LLaMA-3.2 extrapolating Brownian

motion sequences, each generated using a different random seed. As discussed in Section 3.3 and (Liu et al., 2024), the LLM assigns higher influence scores to tokens towards the end of the context window — likely because the earlier portions become increasingly out-of-distribution as the sequence evolves.

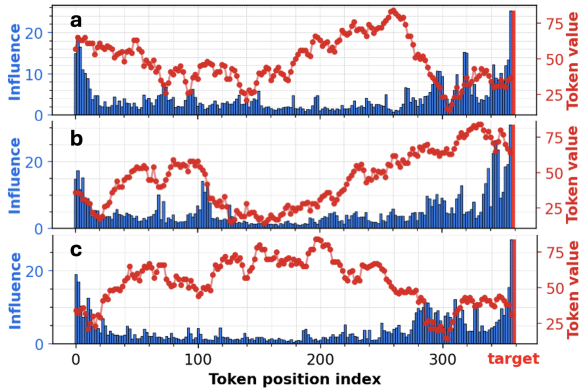


Figure 11: Additional Temperature Scope attributions on LLaMA-3.2 extrapolating Brownian motions in-context.

**LLM attends to spurious patterns in Brownian motion.** Notably, while the overall influence trend increases with context length — as seen in Fig. 11 — there are many abrupt changes and irregularities in the influence score. These anomalies can be explained by random fluctuations: occasionally, patterns or trends may reappear in Brownian motion purely by statistical chance. For instance, in panel (b) of Section 3.3, there is a sudden drop in  $x$ -values around token positions 100, which is “echoed” by a similar drop around the cut-off points at 360. Much like an amateur stock trader who perceives random fluctuations in stock movements as meaningful signals, the LLM incorrectly interprets these coincidental recurrences as informative patterns.

Together, these results illustrate that while LLMs are capable of emergent ICL behaviors such as pattern matching, they may also exhibit human-like tendencies toward superstition (Foster and Kokko, 2009), and perceive spurious patterns in random numerical sequences.

### A.3 Semantic vs. Temperature Scopes

Both Semantic and Temperature Scopes define an influence score via a subspace projection of the input–output Jacobian, as formalized in Eq. (1):

$$\text{Influence}_t := \|\mathbf{v}^\top \mathbf{J}_t\|_2,$$

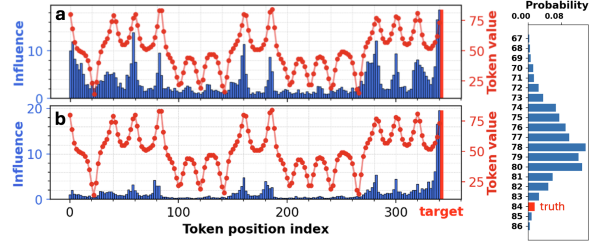


Figure 12: Left: (a) Temperature Scope and (b) Semantic Scope attributions for the same Lorenz system. Right: The predicted probability mass over the top 20 candidate tokens at the target position, ordered by their numerical values. The ground-truth token (shown in red) is used as the target for Semantic Scope.

where the projection direction is chosen as  $\mathbf{v} = \hat{\mathbf{y}}$  for Temperature Scope and  $\mathbf{v} = \mathbf{w}_{\text{target}}$  for Semantic Scope. The distinction therefore lies entirely in the choice of explanandum, i.e. the quantity to be explained: Semantic Scope attributes influence with respect to a single target logit, whereas Temperature Scope attributes influence with respect to the predictive distribution as a whole.

As argued in the main text, Temperature Scope is more appropriate for time-series forecasting tasks, where the object of interest is the full next-step distribution rather than any individual token. We illustrate this distinction with a concrete example in Fig. 12. Conditioned on the first  $T$  inputs, the model’s prediction for the  $(T+1)$ st state exhibits a bell-shaped distribution over approximately 20 numerical tokens, consistent with prior observations in (Liu et al., 2024). The ground-truth value corresponds to only one of many plausible candidates within this distribution.

Naively applying Semantic Scope with the ground-truth token (e.g. “84”) as the target yields misleading attributions: the resulting influence map highlights only the inputs that increase the logit of “84”, while ignoring the remaining tokens that collectively constitute the bell-shaped predictive distribution. As a result, the attribution fails to capture the model’s reasoning at the distributional level. Temperature Scope avoids this failure mode by attributing influence with respect to the predicted distribution as a whole, rather than any single outcome. This makes it better aligned with forecasting settings in which uncertainty and variability are intrinsic to the task.

#### A.4 Fisher vs. Temperature Scopes

Both Fisher and Temperature Scopes attribute input tokens to the full predictive distribution. However, Fisher Scope is substantially more expensive in terms of compute, while also producing cleaner and more interpretable attribution patterns. Fig. 13 illustrates this cost – clarity trade-off by comparing the two Scopes on the same translation task with LLaMA-3.2 1B.



Figure 13: Fisher Scope (top) versus Temperature Scope (bottom) attributions for the same set of translation tasks. For the French example shown, Fisher Scope requires 153 seconds to evaluate, compared to 1.4 seconds for Temperature Scope.

As shown in Fig. 13, Fisher Scope yields highly precise attribution patterns that assign each translated word to its corresponding (sub)word in the source language; for example, *researchers*  $\rightarrow$  *ricercatori*, *attribution*  $\rightarrow$  *Zuschreibung*, and *Scope*  $\rightarrow$  *lentille*. In contrast, Temperature Scope assigns influence more diffusely, highlighting these key source words alongside additional contextual tokens that collectively shape the predictive distribution.

#### A.5 Path-Integrated Semantic Scope

Integrated Gradients (IG) (Sundararajan et al., 2017) is a widely used gradient-based attribution method, with successful applications across computer vision, molecular modeling, and language models. By integrating gradients along a continuous path between a baseline input and the full input, IG aims to mitigate attribution noise arising from non-smoothness (“kinks”) in deep networks. In this section, we compare the original Semantic Scope with its path-integrated analogue and show that, in the LLM setting, IG introduces distortions due to

the out-of-distribution portion of the integration path.

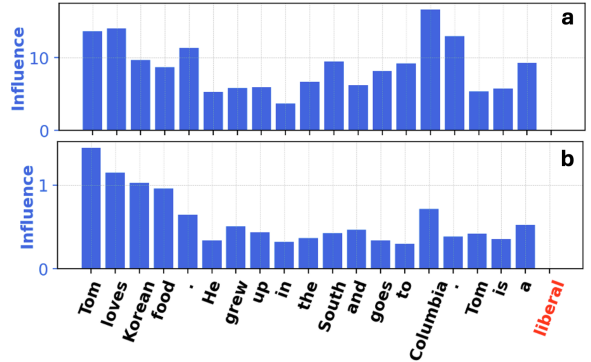


Figure 14: Causal attribution using (a) Semantic Scope and (b) its path-integrated variant based on Integrated Gradients.

To apply Integrated Gradients, one first defines a linear path parameterized by  $\alpha \in [0, 1]$  that connects two matrices  $\mathbf{X} = \mathbf{X}_{1:T}$  and  $\mathbf{X}' = 0$  (the full input and the null baseline):

$$\tilde{\mathbf{X}}(\alpha) = \mathbf{X}' + \alpha(\mathbf{X} - \mathbf{X}').$$

One then selects a scalar output  $z \in \mathbb{R}$  as the explanandum. In our setting,  $\mathbf{X} \in \mathbb{R}^{d_{\text{model}} \times T}$  denotes the full input sequence of token embeddings, and  $z$  is the logit associated with a target vocabulary item (e.g., “*liberal*” or “*conservative*”) <sup>3</sup>.

Consistent with Sundararajan et al. (2017), the Integrated Gradient attribution is defined as

$$\text{IG}(\mathbf{X}) := (\mathbf{X} - \mathbf{X}') \odot \int_0^1 \nabla z(\tilde{\mathbf{X}}(\alpha)) d\alpha, \quad (9)$$

where  $\odot$  denotes element-wise multiplication. This yields an attribution matrix  $\text{IG}(\mathbf{X}) \in \mathbb{R}^{d_{\text{model}} \times T}$ . In direct analogy with Eq. (1), we define the path-integrated influence score for token  $t$  as the  $l^2$ -norm of a vector, namely

$$\text{Influence}_t := \|\text{IG}(\mathbf{X})_t\|_2, \quad (10)$$

where  $\text{IG}(\mathbf{X})_t$  denotes the  $t^{\text{th}}$  column, corresponding to the integrated gradient of the input embedding  $\mathbf{x}_t$ .

Fig. 14 compares the resulting IG attribution with the original Semantic Scope on the example discussed in Section 3.1. Relative to Semantic Scope, the IG-based method assigns disproportionately large influence to early-context tokens,

<sup>3</sup>In the original IG formulation (Sundararajan et al., 2017),  $\mathbf{X}$  represents image pixels and  $z$  corresponds to the logit or log-probability of a predicted class (e.g., “*truck*” or “*boat*”).

thereby obscuring the semantically decisive input token ‘‘Columbia.’’

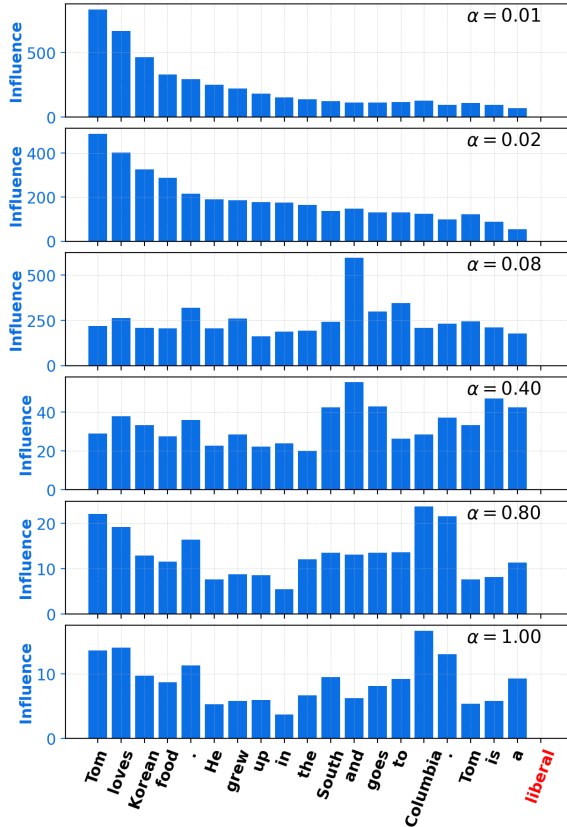


Figure 15: Token-wise  $\ell_2$  norm of the Integrated Gradient integrand  $\nabla z(\tilde{\mathbf{X}}(\alpha))$  along the interpolation path  $\alpha \in [0, 1]$ .

To diagnose the origin of this behavior, we visualize the integrand  $\nabla z(\tilde{\mathbf{X}}(\alpha))$  at several values of  $\alpha$  in Fig. 15. Specifically, for each  $\alpha$  we plot the token-wise  $\ell_2$  norm of the gradient,  $\|\nabla_{\mathbf{x}_t} z(\tilde{\mathbf{X}}(\alpha))\|_2$ , consistent with the influence definition in Eq. (10). In practice, the integral in Eq. (9) is approximated by a discrete sum over 100 uniformly spaced values of  $\alpha$ ; the figure shows a subset of these values.

As a sanity check, we observe that for  $\alpha \rightarrow 1$ , the integrand converges to the Semantic Scope attribution:  $\nabla z(\tilde{\mathbf{X}}(1)) = \nabla z(\mathbf{X})$ . In contrast, at small  $\alpha$  (e.g.,  $\alpha \approx 0.01$ ), the input sequence is nearly indistinguishable from the null input. In this regime, the model operates far outside the data manifold, and circuit-level artifacts dominate. In particular, the ‘‘attention sink’’ phenomenon (Xiao et al., 2024) causes attribution to be overwhelmingly concentrated on early token positions, with influence scores decaying approximately exponentially over context length.

Crucially, the gradient magnitudes in this low- $\alpha$  regime are also large, causing these out-of-distribution effects to dominate the path integral in Eq. (9). At intermediate values of  $\alpha$ , the attribution is often highest for function words such as ‘‘and,’’ which are not semantically relevant to the prediction. Taken together, these observations indicate that the IG path spends substantial measure in regions of representation space that are both out-of-distribution and attributionally pathological.

In summary, while Integrated Gradients can be effective when the interpolation path remains in-distribution, it performs poorly for LLMs. The null-sentence regime introduces severe distortions — most notably attention sink effects — that dominate the attribution signal. Moreover, this degradation comes at a substantial computational cost: in practice, IG requires approximately  $100 \times$  more computation than Semantic Scope due to the discrete approximation of the path integral. As a result, path integration both worsens attribution quality and significantly increases computational overhead in the settings explored in this work.

## A.6 Geometric interpretation of influence under $\varepsilon$ -norm perturbations

We provide a precise justification for the geometric interpretation of the influence score defined in Eq. (1). Recall that  $\mathbf{J}_t := \partial \mathbf{y} / \partial \mathbf{x}_t \in \mathbb{R}^{d_{\text{model}} \times d_{\text{model}}}$  denotes the Jacobian of the leading hidden state  $\mathbf{y}$  with respect to the input embedding  $\mathbf{x}_t$ , and let  $\mathbf{v} \in \mathbb{R}^{d_{\text{model}}}$  denote a fixed direction in output space.

Under a first-order Taylor expansion, a small perturbation  $\delta_t$  to the input embedding induces a change in the output

$$\Delta \mathbf{y} \approx \mathbf{J}_t \delta_t.$$

Projecting this change onto the direction  $\mathbf{v}$  yields the scalar response

$$\mathbf{v}^\top \Delta \mathbf{y} \approx \mathbf{v}^\top \mathbf{J}_t \delta_t.$$

We are interested in the maximum possible change along  $\mathbf{v}$  induced by any perturbation of bounded norm, i.e.,

$$\max_{\|\delta_t\|_2 \leq \varepsilon} \mathbf{v}^\top \mathbf{J}_t \delta_t.$$

By the Cauchy–Schwarz inequality, this quantity is upper-bounded by

$$\mathbf{v}^\top \mathbf{J}_t \delta_t \leq \|\mathbf{v}^\top \mathbf{J}_t\|_2 \|\delta_t\|_2 \leq \varepsilon \|\mathbf{v}^\top \mathbf{J}_t\|_2,$$

with equality achieved when  $\delta_t$  is aligned with  $(\mathbf{v}^\top \mathbf{J}_t)^\top$ . Therefore,

$$\max_{\|\delta_t\|_2 \leq \varepsilon} \mathbf{v}^\top \mathbf{J}_t \delta_t = \varepsilon \|\mathbf{v}^\top \mathbf{J}_t\|_2.$$

This shows that  $\|\mathbf{v}^\top \mathbf{J}_t\|_2$  quantifies the largest possible first-order magnification, along the direction  $\mathbf{v}$ , that can be induced by an  $\varepsilon$ -norm perturbation to the input token embedding  $\mathbf{x}_t$ , up to the scale factor  $\varepsilon$ . This motivates the definition of the influence score in Eq. (1).

### A.7 Second-order KL expansion and Fisher pullback

Let  $\mathbf{p}(\cdot | \mathbf{x}) \in \mathbb{R}^{|\mathcal{V}|}$  denote a smooth family of categorical distributions parameterized by an input  $\mathbf{x}$ . For a small perturbation  $\delta$ , consider the KL divergence

$$\begin{aligned} & \text{KL}(\mathbf{p}(\cdot | \mathbf{x}) \| \mathbf{p}(\cdot | \mathbf{x} + \delta)) \\ &= \sum_i \mathbf{p}(i | \mathbf{x}) \left( \log \mathbf{p}(i | \mathbf{x}) - \log \mathbf{p}(i | \mathbf{x} + \delta) \right). \end{aligned}$$

Under standard regularity conditions, the first-order term vanishes and the KL divergence admits the second-order expansion

$$\text{KL}(\mathbf{p}(\cdot | \mathbf{x}) \| \mathbf{p}(\cdot | \mathbf{x} + \delta)) = \frac{1}{2} \delta^\top \mathbf{F}(\mathbf{x}) \delta + o(\|\delta\|^2),$$

where the Fisher information matrix is given by (Amari and Nagaoka, 2000)

$$\mathbf{F}(\mathbf{x}) := \mathbb{E}_{\mathbf{p}(\cdot | \mathbf{x})}[(\nabla_{\mathbf{x}} \log \mathbf{p})(\nabla_{\mathbf{x}} \log \mathbf{p})^\top].$$

For a categorical distribution parameterized by logits  $\mathbf{z} \in \mathbb{R}^{|\mathcal{V}|}$  with  $\mathbf{p} = \text{softmax}(\mathbf{z})$ , the Fisher information with respect to  $\mathbf{z}$  takes the closed form (Bishop and Nasrabadi, 2006)

$$\mathbf{F}_z = \text{Diag}(\mathbf{p}) - \mathbf{p}\mathbf{p}^\top.$$

If the logits are given by  $\mathbf{z} = \mathbf{W}\mathbf{y}$ , then the Fisher information with respect to the hidden state  $\mathbf{y}$  is

$$\mathbf{F}_u = \mathbf{W}^\top (\text{Diag}(\mathbf{p}) - \mathbf{p}\mathbf{p}^\top) \mathbf{W}.$$

### A.8 Expected KL under isotropic unit-norm perturbations

Consider the local quadratic expansion

$$\text{KL}(\mathbf{p}(\cdot | \mathbf{x}) \| \mathbf{p}(\cdot | \mathbf{x} + \delta)) = \frac{1}{2} \delta^\top \mathbf{F}_t \delta + o(\|\delta\|^2)$$

and isotropic unit-norm perturbations  $\delta = \varepsilon \mathbf{u}$ , where  $\varepsilon > 0$  is small and  $\mathbf{u} \in \mathbb{R}^d$  is uniform on the unit sphere ( $\|\mathbf{u}\|_2 = 1$ ). Taking expectation and using  $\mathbb{E}_{\mathbf{u}}[\mathbf{u}\mathbf{u}^\top] = \frac{1}{d}\mathbf{I}$  yields

$$\begin{aligned} & \mathbb{E}_{\mathbf{u}}[\text{KL}(\mathbf{p}(\cdot | \mathbf{x}) \| \mathbf{p}(\cdot | \mathbf{x} + \varepsilon \mathbf{u}))] \\ &= \frac{1}{2} \varepsilon^2 \mathbb{E}_{\mathbf{u}}[\mathbf{u}^\top \mathbf{F}_t \mathbf{u}] + o(\varepsilon^2) \\ &= \frac{1}{2} \varepsilon^2 \text{tr}(\mathbf{F}_t \mathbb{E}_{\mathbf{u}}[\mathbf{u}\mathbf{u}^\top]) + o(\varepsilon^2) \\ &= \frac{1}{2} \varepsilon^2 \frac{1}{d} \text{tr}(\mathbf{F}_t) + o(\varepsilon^2). \end{aligned} \quad (11)$$

Thus, up to the universal factor  $\varepsilon^2/(2d)$ , the trace  $\text{tr}(\mathbf{F}_t)$  governs the expected KL divergence induced by an isotropic unit-norm perturbation of the input.